Optically Active Perovskite CsPbBr 3 Nanocrystals Helically Arranged on Inorganic Silica Nanohelices

Peizhao Liu, Wei Chen, Yutaka Okazaki, Yann Battie, Lysiane Brocard, Marion Decossas, Emilie Pouget, Peter Müller-Buschbaum, Brice Kauffmann, Shaheen Pathan, et al.

Optically Active Perovskite $CsPbBr_3$ Nanocrystals Helically Arranged on Inorganic Silica Nanohelices

Peizhao Liu,[1, 2] Wei Chen,[5] Yutaka Okazaki,[2] Yann Battie,[3] Lysiane Brocard,[4] Marion Decossas[1], Emilie Pouget[1], Peter Müller-Buschbaum,[5, 6] Brice Kauffmann,[7] Shaheen Pathan,[1] Takashi Sagawa,*[2] and Reiko Oda*[1]

[1]Chimie et Biologie des Membrance et des Nanoobjets (CBMN), CNRS, University of Bordeaux, Bordeaux INP, UMR 5248, 33607, Pessac, France

[2]Graduate School of Energy Science, Kyoto University, 606-8501, Kyoto, Japan

[3] Laboratoire de Chimie et Physique - Approche Multi-échelles des milieux Complexes, (LCP-A2MC), Université de Lorraine, 1 Boulevard Arago, 57078 Metz, France.

[4] Bordeaux Imaging Centre, Plant Imaging Plateform, UMS 3420, INRA-CNRS-INSERM-University of Bordeaux, 71 Avenue Edouard Bourlaux, 33883 Villenave-d'Ornon Cedex, France

[5] Physik Department, Lehrstuhl für Funktionelle Materialien, Technische Universität München, James-Franck-Straße 1, 85748 Garching, Germany.

[6] Heinz Maier-Leibnitz Zentrum (MLZ), Technische Universität München, Lichtenbergstraße. 1, 85748 Garching, Germany

[7] Institut Européen de Chimie et Biologie (UMS 3033), Université de Bordeaux–CNRS-INSERM 2 rue Robert Escarpit, 33607 Pessac, France.

KEYWORDS. Silica nanohelices, Perovskite nanocrystals, Chirality Induction, Circular dichroism and circularly polarized luminescence

ABSTRACT.

Perovskite nanocrystals (PCNs) exhibited excellent absorption and luminescent optical properties. Inorganic silica nanohelices are used as chiral templates to induce optically active properties to $CsPbBr_3$ PNCs grafted on their surfaces. In suspension, PNCs synthesized and grafted on the right (or left) handed silica helices do not show any detectable chiroptical properties. In contrast, in a dried film state, they show large circular dichroism (CD) and circularly polarized luminescence (CPL) signals with dissymmetric factor up to $6*10^{-3}$. Grazing incidence X-ray scattering, tomography electron microscopy (EM) and cryo EM have shown closely and helically packed PNCs if the nanohelices@PNCs are dried in contrast to much more loosely organized PNCs solvated in suspension. Simulations based on the coupled dipole method (CDM) demonstrate that the CD comes from the dipolar interaction between PNC assembled into a chiral structure. We show that the CD decreases as the interparticle distance increases. These results indicate that closely packed and helically arranged PNCs on silica nanohelices result in an increase of the optically active properties in the film state.

INTRODUCTION

Recently, the optically active (OA) properties of semiconductor nanocrystals (SNCs) have attracted large attention due to the outstanding properties of SNCs[1-3] and prospective applications in chiral separation and recognition, chiral catalysis, and 3 D display technology.[4-6] Generally, there are four ways to endow chirality to SNCs: i) Combination with chiral ligands;[7, 8] ii) chiral shape of the individual NC;[9] iii) formation of a chiral lattice;[10] and iv) chiral arrangement in the presence of chiral building blocks.[11, 12] In the past decades, SNCs with chiral ligands have been widely reported for the induction of circular dichroism (CD) signals [13-16], whereas a much more limited number of reports can be found for the induction of circularly polarized luminescence (CPL)[17, 18] due to the lower photoluminescence quantum yield (PLQY) after ligand exchange.[19-21] Core shell structure SNCs could boost the PLQY, but the outer shell decreases the chirality induction resulting in a lower dissymmetric g-factor.[22] The typical absorption and luminescence dissymmetric factors (g) were reported in the range of 10^{-5} to 10^{-3}. Only with chiral HgS SNCs synthesized with chiral ligands, dissymmetric factors as large as 10^{-2} were achieved.[23] From the chiral lattice formation or chiral shape of SNCs, only induced CD (ICD) and no induced CPL (ICPL) were reported so far.

SNCs could be self-organized directly into chiral superstructure driven by chiral ligands, oxidation, pH controlling or under circularly polarized light illumination.[24-26] SNCs self-organization could also happen with chiral organic molecular self-assembly as soft templates, big CPL could be observed. However, such SNCs chiral self-organization could be easily destroyed by changing the temperature due to the fragile nature of the organic molecular self-assembly.[12, 27] Inorganic chiral templates offer more robust and promising alternatives. For example, Che reported chirality introduction by a metal ions or metal oxides chiral arrangement with the chiral

mesoporous silica due to molecular imprinting.[28] In our previous work,[29, 30] gold nanoparticles electrostatically adsorbed or covalently grafted on the surface of silica nanohelices also showed strong CD signals from their plasmonic resonance. The constituents of these systems were totally inorganic, allowing them to be dispersed in a large range of solvents, withstand drying and flow induced organization enhancing the optical properties of the system.

Herein, pure enantiomer (right handed or left handed) inorganic silica nanohelices and perovskite $CsPbBr_3$ nanocrystals (PNCs) are chosen for the inorganic building blocks. First, the surface of silica helices is modified with amine by 3-aminopropyl-triethoxysilane (APTES). Then the PNCs are grafted on the surface of silica helices by a ligand exchange method. Unlike our previous result of gold nanoparticle combined with silica nanohelices,[29] the PNCs grafted on silica helices do not show observable CD signals or CPL signals when suspended in solvent (toluene). However, surprisingly strong CD and CPL signals are observed after the suspension of nanohelices with PNCs are drop cast to create a dry film. The organization of the PNCs on the silica helices both in dried film and in suspension, are evaluated with grazing incident x-ray scattering (GIXS), tomography electron microscopy and cryo EM. Closely packed and helically arranged PNCs are observed for the dried film whereas loosely attached PNCs with much less coherent periodic organization likely due to the ligand solvation was observed for the solvated helices. Simulations based on the coupled dipole method (CDM), demonstrate that the CD is related to the dipolar interaction between PNCs assembled into a chiral structure. The amplitude of the simulated CD spectra strongly depends both on the grafting density of the PNCs and on their interparticle distance. These results indicate that closely packed and helically arranged PNCs on the silica nanohelices formed during the drying lead to the strong OA properties in the film state whereas OA properties are not observable for the solvated loosely packed PNCs with larger mean distances

on nanohelices as the electromagnetic interaction between PNCs fades away quickly with the interparticle distances. Such observation can help achieving optically active functional materials with an all inorganic building block system. The temperature stability of the PNCs-silica nanohelices film has also been evaluated. The CD dissymmetric g-factor is unchanged upon heating to 80 °C.

RESULT AND DISCUSSION

As in our previous reports, the synthesis of right or left handed silica nanohelices were performed using cationic bis-quaternary ammonium gemini surfactants of chemical formula C_2H_4-1,2-$((CH_3)_2N^+C_{16}H_{33})_2$, noted hereafter 16-2-16, which self-assemble in water to form nanometric helical structures in the presence of tartrate counterions. With L tartrate, right handed helices are formed and with D tartrate, left handed helices are formed.[31, 32] The resulting organic nanohelices were used as templates for the sol−gel condensation of a tetra alkoxysilane to obtain silica nanohelices.[33, 34] The organic helices were then washed away with methanol and the obtained silica nanohelices can be further functionalized by APTES. The Figures 1 (a) and (b) show the scanning electron microscope (SEM) images of the right handed and left handed silica nanohelices respectively. Detailed information about the silica nanohelix is shown in S1. |The width and the pitch of silica helix are about 30 nm and 60 nm, respectively. The Figure 1 (c) shows the transmission electron microscope (TEM) image of PNCs. The surface of colloidal nanocrystals in suspension as prepared as described in the supporting information is covered with ligands which are in equilibrium with those in solution.[35] The PNCs in toluene suspension as used in this study are covered with two types of ligands: oleic acid (bound to cations of Cs or Pb) and oleylamine (bound to halide anions). This bonding between ligands and PNCs also shows a dynamic

equilibrium as depicted in Figures 1 (d) and (e). The PNCs have cubic shape with an average size of 9.5 nm (Figure S2 (a)), with a small peak at 474 nm in the UV-vis range (Figure S2 (b)). When PNCs are drop-cast on the surface of quartz and dried at 20 °C, as shown in figure S3, the film show strong angle dependent LDs, which suggested their strong tendency for self-organization during the solution evaporation process.[36]

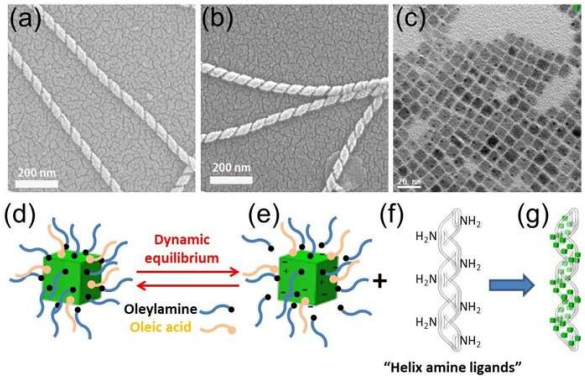

Figure 1. SEM images of (a) right handed silica helices, (b) left handed silica helices and (c) TEM image of PNCs. (d)-(g) Scheme of the ligands exchange grafting method as discussed in the text.

When the PNCs and amine modified silica nanohelices (Figure 1 (f)) were mixed together, the PNCs were grafted homogeneously on the surface of silica nanohelices as shown in Figures 2 (a) and (b) from the cryogenic electron microscopy (cryo-EM) images taken in toluene. This is likely due to the ligands exchange between the oleylamine and "helix amine ligands" as shown in Figure 1 (g). In contrast with our previous observations with gold nanoparticles@silica nanohelices[29], no CD or CPL are observed from these suspensions (Figures 2 (c) and (d)). The absorption spectra (Figure 2 (c)) indicated that PNCs-$CsPbBr_3$–silica nanohelices show broad absorption with

absorption peak at around 500 nm which is slightly red shifted as compared with that of PNCs (Figure S2 (b)). This red shift might correspond to the exciton coupling between grafted PNCs or the increasing size of the PNCs (aggregation) during the mixing and grafting process.[37, 38] The cryo-EM image of solvated PNCs-L-silica nanohelices show that there are no free PNCs which remain in solution.

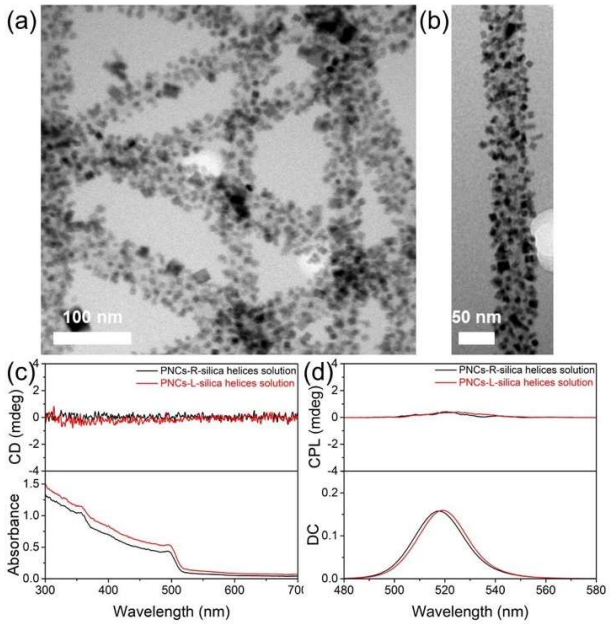

Figure 2. (a) and (b) Cryo-EM images of PNCs-L-silica nanohelices in toluene, (c) UV-Vis absorbance and CD spectra and (d) fluorescence (Ex@ 365 nm) and CPL spectra of PNCs-R-silica nanohelices (black) and PNCs-L-silica nanohelices (red)

The PNCs-R/L-silica nanohelices films were made by drop casting PNCs-R/L-silica nanohelices suspension (50 µl of 20 mg/ml suspension) on the surface of quartz and drying them at 4 °C or 20 °C. Strong CD and CPL signals are observed as shown in Figures 3 (b) and (c) as well as Figures S5 and S6. For the films dried at 4 °C, the right-handed PNCs-R-silica nanohelices show a positive

CD signal with the maximum g_{abs} ~$6.2*10^{-3}$ at around 367.5 nm whereas the left-handed PNCs-L-silica nanohelices show a negative CD signal with g_{abs} ~-$6.4*10^{-3}$. Tomography TEM image with 3D reconstruction of the dried (@20 °C) sample is shown in Figure 3 (a). It is clearly observed that compared with the solvated cryo-EM image, the grafted PNCs of the dried sample are closer to the surface of silica helices and the reconstituted images (framed in red and yellow) clearly show a helical arrangement of the PNCs along the helical ribbons. This is likely due to the ligands collapse while solvent evaporation and rearrangement of the PNCs during the drying process. These PNCs probably have a much stronger local interaction and organization with the small surface area on the silica nanohelices.

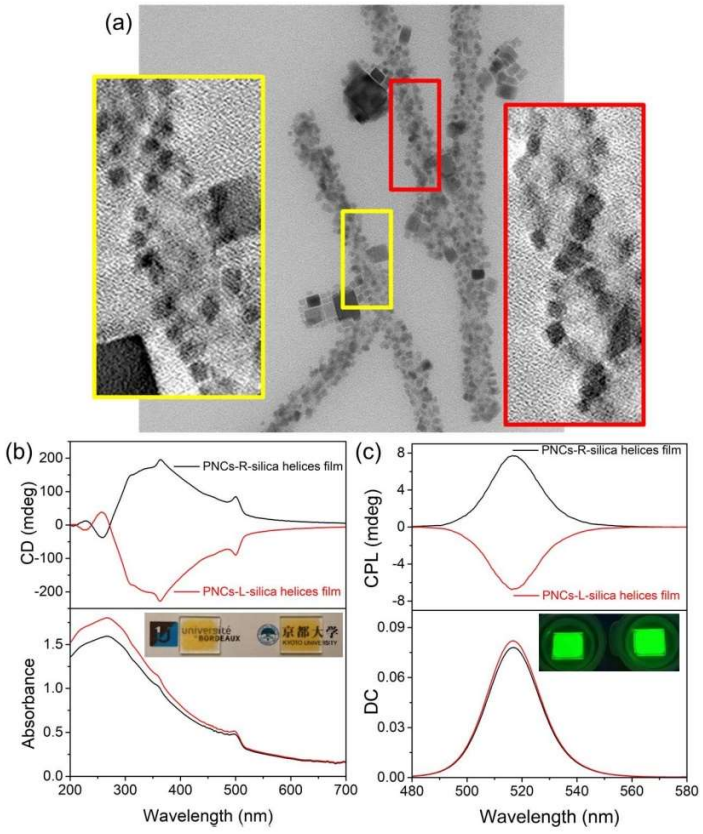

Figure 3. (a) TEM image of nanohelices@PNCs and the cross-sections obtained with the tomography 3D reconstructions (framed in red and yellow) for dried film. (b) Absorbance and CD spectra and (c) DC and CPL spectra of PNCs-R-silica nanohelices (black) and PNCs-L-silica nanohelices film (red) dried at 4 °C. The inset picture in (b) shows the drop-caste film from right handed and left handed samples under natural light. The inset picture in (c) shows the drop-cast films from right handed and left handed samples irradiated under a UV lamp at 365 nm. The mean values of data measured at 0° and 90° are shown in order to eliminate the contribution of linear dichroism. The dissymmetric factors for PNCs-L/R-silica helices are g_{abs} ($_{abs}$367.5 nm) ~6.2*10^{-3}/-6.4*10^{-3} and g_{lum} ($_{em}$517.5 nm) ~6.9*10^{-3}/-5.7*10^{-3}.

The LD of the films are negligible in the wavelength range beyond 350 nm. The inset picture in Figure 3(b) shows that the films have good transparency under natural light as the university logos can still be observed through the films. The CPL spectra also show mirror images and the maximum g_{lum} at 517.5 nm are 6.9*10^{-3} for PNCs-R-silica nanohelices and -5.7*10^{-3} for PNCs-L-silica nanohelices respectively. For the film dried at 20 °C, the dissymmetric g-factor of CD and CPL (around 3-4*10^{-3}) are smaller (Figures S5 and S6). Previously, Bodnarchuk *et al.* reported that the temperature had an important effect on the nanocrystals self-organization.[39] Recently, Rebecca et al. also reported that the solvent evaporation speed control the perovskite nanoplatelets orientation (edge-up or face-down).[40] Therefore, the difference of the dissymmetric g-factor of CD and CPL at different drying temperature can be attributed to these effects.

The evolution of the CD or CPL signals during the drying process is investigated as follows: First PNCs-R/L-silica nanohelices suspension was dried on a quartz at 20 °C to create films. Then 10 μL toluene was added on the surface of the film in order to soak the silica nanohelices. The CD

and LD spectra of such wetted film is measured at 502 nm during drying at various temperatures (0 – 80°C) as shown in Figure S7. Upon soaking with toluene, the CD value decreased from initial ~ ±40 mdeg (measure as dried film with R- and L- silica nanohelices) to ~±7 mdeg (measured at t=0). Here, we should note that once a dried film is formed, adding toluene to wet the film does not transform the sample totally back to the original suspension state and the CD value @502 nm does not totally diminish to ~0 mdeg. During the initial stage of toluene evaporation at various temperatures, the CD values do not vary significantly. Then at a given time which depends on the temperature, a sudden increase of the CD value is observed, followed by reaching a plateau. Interestingly, the final CD values are higher for the samples dried at lower temperature in agreement with our observation in Figure S5, and S6. The CPL signal also shows a similar kinetic behavior as the CD (Figure S8). Weidman, Tisdale *et al.* reported that the drying of a free nanocrystals suspension in toluene to a solid state PbS nanocrystal film resulted in a self-organization as observed by *in-situ* Grazing Incident X-ray Scattering.[41] The free nanocrystals show superstructure formation within 1-2 minutes during drying process. A superstructure formation of the PNCs of cesium lead halide by self-organization was also observed during the evaporation process.[42]

The local organization of PNCs in the dried samples is investigated with grazing incidence small angle X-ray scattering (GISAXS).[43] Samples which were dried at 4°C and 20 °C, are compared mainly based on the horizontal line-cut analysis as shown in figure 4. These data are analyzed with a modeling as described in the supporting information (Figure S10 and table S2). The modeling results indicate that the 4 °C dried film has a smaller interparticle distance (11 ± 2 nm) than the dried one (12 ± 2 nm), which suggests the PNCs coupling in 4 °C dried film is stronger than that in the 20 °C dried one. Moreover, the GISAXS line-cut of the 20 °C dried film exhibits a prominent

shoulder at a large q_y range, which is attributed to the presence of PNCs clusters (or aggregates). Solvent evaporation at 20 °C shortens the self-organization time of the PNCs as comparing with the time available in the 4 °C condition, thereby leading to the formation of the PNCs aggregates. The as-formed aggregates are likely to cause an inhomogeneous coupling to the remaining PNCs ensemble.[44] The intensity contribution from the aggregates in the 4 °C case is relatively weak indicating a homogeneous PNCs arrangement. Consequently, a uniform PNCs-coupling is expected in the 4 °C dried film. Notably, the effective 3D substrate by the silica nanohelices, as shown in Figure 4(d), leads to a smeared feature of the PNCs interparticle distance. The grazing incidence wide angle X-ray scattering (GIWAXS) data as shown in Figure S11 reveal the anisotropic orientation distribution for all Bragg peaks in PNCs-silica nanohelices films. This observation is a direct indication of the successful grafting of the effective 3D substrate (silica nanohelices) and the PNCs are homogeneously distributed on the 3D surface.

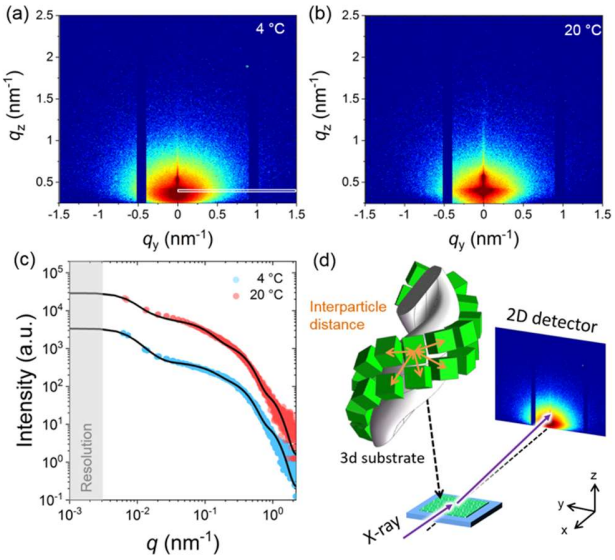

Figure 4. 2 D GISAXS data of PNCs-R-silica nanohelices films dried at (a) 4 ℃ and (b) 20 °C. (c) Horizontal line cut data of films dried at 4 °C (blue) and 20 °C (red) shown with fit (solid lines)

based on a model as explained in the supporting information. (d) Schematic of the GIXS experiment for analysis of the imprinting on PNCs-silica nanohelices, in which the silica nanohelices act as an effective 3D substrate leading to a smeared scattering feature of the PNCs interparticle distance.

The optical properties of a PNCs-silica nanohelix are simulated by using the coupled dipole method (CDM) as described in the supporting information. Figure 5(a) shows a schematic representation of the models used for the simulation, which consist of helically ordered PNCs. Figure 5(b) shows the influence of the density of the PNCs by removing various percentages of PNCs from the perfect alignment. As it is clearly visible, simulated CD spectra exhibit the same spectral variations as the measured ones (Figure 3(a)), suggesting that the CD signal comes from the interaction between the induced dipoles. The amplitude of the CD and g-factor spectra decrease as the amount of removed PNC increases. As it is can be observed with tomography TEM, the organization of the PNCs are not exactly as it is in the model. There are some domains where we observe closely packed and helically arranged PNCs, but there are other areas where the arrangement is not that perfect. Therefore, we evaluated the effect of defect by removing randomly various percentage of PNCs. The g-factors calculated from these plots shows that the observed g-factor @516 nm simulates the best match when around 30% of PNCs are removed with the interparticle 1 nm. The CD is negligible for higher wavelength than 550 nm, while it progressively increases as the wavelength decreases. The CD reaches its maximum value at 325 nm. According to simulations proposed by Kovalenko et al.,[1] the bands located at 516 nm and 325 nm can be related to the lowest-energy excitonic transition at R point of the first Brillion zone (BZ) and the

second lowest energy transition at the M point of BZ, respectively. The inset in the Figure 5(b) illustrates the influence of the interparticle distance on the CD and g-factor of a single NPC-silica nanohelix. The CD signal and g-factor decreases as the interparticle distance increases. Indeed, the g-factor decreases by half when the interparticle distance is increased from 1 to 2 nm, then continues to decrease. Beyond 4 nm, it is less than 10 % of the initial value. It is clearly observed that the amplitude of the scattered field decreases with the distance from the PNC dipole source. Therefore, the interaction between PNCs and the CD become negligible for large interparticle distances.

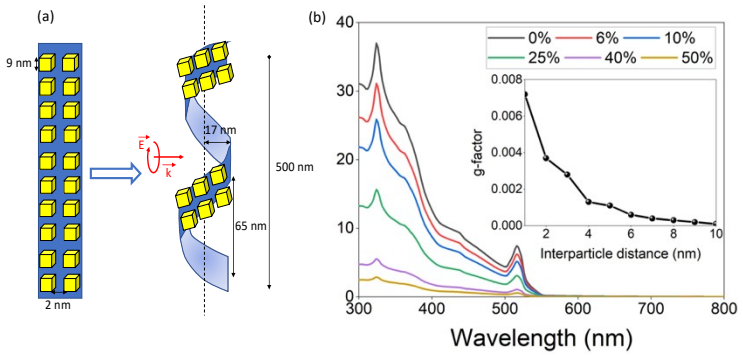

Figure 5. (a) Schematic representation of helically ordered PNCs. All simulations are performed by considering a NPCs size of 9 nm. Two rows of PNCs are perfectly aligned around the helix, the radius of the helix is 34 nm, and the pitch is 65 nm (b) Simulated CD of a PNC-silica helix for several amount of randomly removed NPCs. In inset of (b), the evolution of the g-factor at a 516 nm wavelength with the interparticle distance (1-10 nm) is simulated by removing 30% of NPCs (which gives the g-factor as observed experimentally in dried sample).

Such observations are in very good agreement with the effect of drying vs solvated samples as well as the effect of the drying temperature on the g-factors. The comparison between cryo-EM

(solvated) and tomography TEM (dried) show clearly that PNCs are closely attached to the silica nanohelices and also are close with each other probably due to the collapse of the ligands when dried. SAXS measurements (figure S13) show that there is no interparticle correlation when the nanohelices are solvated whilst for the dried samples, correlation distances with the particle-to-particle distances of 1-2 nm (drying temperature of 4°C and 20°C respectively) are observed. The variation of the simulated g-factor is in good agreement with the measured ones during the drying process. We conclude that having no correlation distance (no self-organization) and an increasing interparticle distance of the PNCs are likely the origin of the disappearing of the CD signals for the solvated samples. This result is in contrast with our previous report on gold nanoparticles (GNPs) grafted on silica nanohelices which showed induced CD even when suspended in water. Indeed, the difference comes from the range of induced electromagnetic field between GNPs and PNCs. Indeed, contrary to PNCs, the polarizability of GNPs reaches a maximum value at the plasmon resonance energy. As a consequence, the scattered electric field by GNPs is enhanced and has a higher magnitude than the scattered field by PNCs and has a longer range.

The temperature stability of the CD or CPL signals of the PNCs-R/L-silica nanohelices films is evaluated as well. The g_{abs} and g_{lum} spectra of PNCs-R/L-silica nanohelices in the temperature ranging between 0 °C and 90 °C (g_{abs}) and -10 to 80 °C (g_{lum}) are shown in Figures S15. The spectra of PNCs-L/R-silica nanohelices are shown in Figure S14. While the g_{abs} show almost no variation with temperature upon heating and cooling, g_{lum} is less stable upon heating as the emission intensity decreased to less than 10% of the initial intensity. Upon cooling, the emission intensity recovered slightly (~35% of the initial intensity) but not totally as shown in Figure S16, probably due to the thermal photoluminescence quenching, as previously reported.[45]

CONCLUSION

Perovskite $CsPbBr_3$ nanocrystals are grafted on the surface of silica nanohelices by a ligand exchange method. In toluene suspension, such PNC grafted silica nanohelices do not show any observable optical activity. After drying on substrates to form films, strong CD and CPL signals are observed with the dissymmetric factor of $> 6*10^{-3}$. Solvated and dried TEM images both show densely attached PNCs on the surface of the nanohelices. However, for the solvated nanohelices, the PNCs show a thicker and swollen layer around the silica nanohelices without detectable helical organization probably with strongly solvated ligands. In contrast, for the dried nanohelices, the PNCs are closely attached on the surface, suggesting ligands collapse and a higher interaction between the both, which may induce higher self-organization with a 3 dimensional spiral arrangement of the PNCs along with the inorganic chiral silica nanohelices. GISAXS confirms a correlation between PNCs for the dried samples, which does not exist for solvated samples. CDM simulation clearly confirm that for the dielectric nanoparticles such as PNCs, the correlation between the particles to "feel" the chirality, the interparticle distances need to be very close to each other with good alignment, which is likely why solvated samples with larger particle distances with much less ordered organization do not show any detectable CD. This result is in contrast with our previous report on gold nanoparticles for which the electromagnetic field has longer range. The samples dried at 4 °C (with slower drying) show stronger ICD signals than those dried at 20 °C (faster drying), which is probably due to the closer packing originating from the slower film drying. The films show an excellent photostability in their absorbance and CD properties, however, loose strongly their emissivity upon heating up to 80 °C.

AUTHOR INFORMATION

Corresponding Author

*Email: r.oda@cbmn.u-bordeaux.fr

*Email: sagawa.takashi.6n@kyoto-u.ac.jp

Author Contributions

The manuscript was written through contributions of all authors. All authors have given approval to the final version of the manuscript.

Funding Sources

This work was supported by the France-Japan International Associated Laboratory, Chiral Nanostructures for Photonic Applications (LIA-CNPA) as well as the Centre National de la Recherche Scientifique and Université de Bordeaux. Y.O. acknowledges the JSPS Overseas Research Fellowship. P.M.-B. funding by the Deutsche Forschungsgemeinschaft (DFG, German Research Foundation) under Germany´s Excellence Strategy – EXC 2089/1 – 390776260 (e conversion). P.L. and W.C. are grateful for financial support from the Chinese Scholarship Council (CSC).

Notes

The authors declare no competing financial interest.

REFERENCES

(1) Protesescu, L.; Yakunin, S.; Bodnarchuk, M. I.; Krieg, F.; Caputo, R.; Hendon, C. H.; Yang, R. X.; Walsh, A.; Kovalenko, M. V. Nanocrystals of cesium lead halide perovskites ($CsPbX_3$, X= Cl, Br, and I): novel optoelectronic materials showing bright emission with wide color gamut.

Nano Lett. **2015,** *15*, 3692-3696.

(2) Li, X.; Wu, Y.; Zhang, S.; Cai, B.; Gu, Y.; Song, J.; Zeng, H. $CsPbX_3$ Quantum Dots for Lighting and Displays: Room-Temperature Synthesis, Photoluminescence Superiorities, Underlying Origins and White Light-Emitting Diodes. *Adv. Funct. Mater.* **2016,** *26*, 2435-2445.

(3) Liu, P.; Chen, W.; Wang, W.; Xu, B.; Wu, D.; Hao, J.; Cao, W.; Fang, F.; Li, Y.; Zeng, Y.; Pan, R.; Chen, S.; Cao, W.; Sun, X. W.; Wang, K. Halide-Rich Synthesized Cesium Lead Bromide Perovskite Nanocrystals for Light-Emitting Diodes with Improved Performance. *Chem. Mater.* **2017,** *29*, 5168-5173.

(4) Gao, X.; Han, B.; Yang, X.; Tang, Z. Perspective of Chiral Colloidal Semiconductor Nanocrystals: Opportunity and Challenge. *J. Am. Chem. Soc.* **2019,** *141*, 13700-13707.

(5) Wang, C. T.; Chen, K.; Xu, P.; Yeung, F.; Kwok, H. S.; Li, G. Fully chiral light emission from $CsPbX_3$ perovskite nanocrystals enabled by cholesteric superstructure stacks. *Adv. Funct. Mater.* **2019**, 29, 1903155.

(6) Long, G.; Sabatini, R.; Saidaminov, M. I.; Lakhwani, G.; Rasmita, A.; Liu, X.; Sargent, E. H.; Gao, W. Chiral-perovskite optoelectronics. *Nat Rev Mater* **2020**, 5, 423-439.

(7) Ben Moshe, A.; Szwarcman, D.; Markovich, G. Size dependence of chiroptical activity in colloidal quantum dots. *ACS nano* **2011,** *5*, 9034-9043.

(8) Zhou, Y.; Zhu, Z.; Huang, W.; Liu, W.; Wu, S.; Liu, X.; Gao, Y.; Zhang, W.; Tang, Z. Optical coupling between chiral biomolecules and semiconductor nanoparticles: size-dependent circular dichroism absorption. *Angew. Chem. Int. Ed.* **2011,** *50*, 11456-11459.

(9) Ben-Moshe, A.; Wolf, S. G.; Bar Sadan, M.; Houben, L.; Fan, Z.; Govorov, A. O.; Markovich, G. Enantioselective control of lattice and shape chirality in inorganic nanostructures using chiral biomolecules. *Nat. Commun.* **2014,** *5*, 4302.

(10) Ben-Moshe, A.; Govorov, A. O.; Markovich, G. Enantioselective synthesis of intrinsically chiral mercury sulfide nanocrystals. *Angew. Chem. Int. Ed.* **2013,** *52*, 1275-1279.

(11) Huo, S.; Duan, P.; Jiao, T.; Peng, Q.; Liu, M. Self-Assembled Luminescent Quantum Dots To Generate Full-Color and White Circularly Polarized Light. *Angew. Chem. Int. Ed.* **2017,** *56*, 12174-12178.

(12) Shi, Y.; Duan, P.; Huo, S.; Li, Y.; Liu, M. Endowing perovskite nanocrystals with circularly polarized luminescence. *Adv. Mater.* **2018,** *30*, 1705011.

(13) Choi, J. K.; Haynie, B. E.; Tohgha, U.; Pap, L.; Elliott, K. W.; Leonard, B. M.; Dzyuba, S. V.; Varga, K.; Kubelka, J.; Balaz, M. Chirality Inversion of CdSe and CdS Quantum Dots without Changing the Stereochemistry of the Capping Ligand. *ACS Nano* **2016,** *10*, 3809-3815.

(14) Gao, X.; Zhang, X.; Deng, K.; Han, B.; Zhao, L.; Wu, M.; Shi, L.; Lv, J.; Tang, Z. Excitonic Circular Dichroism of Chiral Quantum Rods. *J. Am. Chem. Soc.* **2017,** *139*, 8734-8739.

(15) Gao, X.; Zhang, X.; Zhao, L.; Huang, P.; Han, B.; Lv, J.; Qiu, X.; Wei, S. H.; Tang, Z. Distinct Excitonic Circular Dichroism between Wurtzite and Zincblende CdSe Nanoplatelets. *Nano Lett.* **2018,** *18*, 6665-6671.

(16) Govorov, A. O.; Fan, Z.; Hernandez, P.; Slocik, J. M.; Naik, R. R. Theory of circular dichroism of nanomaterials comprising chiral molecules and nanocrystals: plasmon enhancement, dipole interactions, and dielectric effects. *Nano Lett.* **2010,** *10*, 1374-1382.

(17) Cheng, J.; Hao, J.; Liu, H.; Li, J.; Li, J.; Zhu, X.; Lin, X.; Wang, K.; He, T. Optically Active CdSe-Dot/CdS-Rod Nanocrystals with Induced Chirality and Circularly Polarized Luminescence. *ACS Nano* **2018,** *12*, 5341-5350.

(18) Tohgha, U.; Deol, K. K.; Porter, A. G.; Bartko, S. G.; Choi, J. K.; Leonard, B. M.; Varga, K.; Kubelka, J.; Muller, G.; Balaz, M. Ligand induced circular dichroism and circularly polarized

luminescence in CdSe quantum dots. *ACS nano* **2013,** *7*, 11094-11102.

(19) Osaki, F.; Kanamori, T.; Sando, S.; Sera, T.; Aoyama, Y. A quantum dot conjugated sugar ball and its cellular uptake. On the size effects of endocytosis in the subviral region. *J. Am. Chem. Soc.* **2004,** *126*, 6520-6521.

(20) Gao, X.; Chan, W. C.; Nie, S. Quantum-dot nanocrystals for ultrasensitive biological labeling and multicolor optical encoding. *J.biomed. opt.* **2002,** *7*, 532-538.

(21) William, W. Y.; Chang, E.; Drezek, R.; Colvin, V. L. Water-soluble quantum dots for biomedical applications. *Biochem. Biophys. Res. Commun.* **2006,** *348*, 781-786.

(22) Purcell-Milton, F.; Visheratina, A. K.; Kuznetsova, V. A.; Ryan, A.; Orlova, A. O.; Gun'ko, Y. K. Impact of Shell Thickness on Photoluminescence and Optical Activity in Chiral CdSe/CdS Core/Shell Quantum Dots. *ACS Nano* **2017,** *11*, 9207-9214.

(23) Wang, P. P.; Yu, S. J.; Govorov, A. O.; Ouyang, M. Cooperative expression of atomic chirality in inorganic nanostructures. *Nat. Commun.* **2017,** *8*, 14312.

(24) Feng, W.; Kim, J.-Y.; Wang, X.; Calcaterra, H. A.; Qu, Z.; Meshi, L.; Kotov, N. A. Assembly of mesoscale helices with near-unity enantiomeric excess and light-matter interactions for chiral semiconductors. *Sci. adv.* **2017,** *3*, e1601159.

(25) Yeom, J.; Yeom, B.; Chan, H.; Smith, K. W.; Dominguez-Medina, S.; Bahng, J. H.; Zhao, G.; Chang, W.-S.; Chang, S.-J.; Chuvilin, A.; Melnikau, D.; Rogach, AL.; Zhang, P.; Link, S.; Krái, P.; Kotov, N. A. Chiral templating of self-assembling nanostructures by circularly polarized light. *Nat. mater.* **2015,** *14*, 66-72.

(26) Zhou, Y.; Marson, R. L.; van Anders, G.; Zhu, J.; Ma, G.; Ercius, P.; Sun, K.; Yeom, B.; Glotzer, S. C.; Kotov, N. A. Biomimetic Hierarchical Assembly of Helical Supraparticles from Chiral Nanoparticles. *ACS Nano* **2016,** *10*, 3248-3256.

(27) Han, J.; You, J.; Li, X.; Duan, P.; Liu, M. Full-Color Tunable Circularly Polarized Luminescent Nanoassemblies of Achiral AIEgens in Confined Chiral Nanotubes. *Adv. Mater.* **2017,** *29*, 1606503.

(28) Duan, Y.; Che, S. Electron transition-based optical activity (ETOA) of achiral metal oxides derived from chiral mesoporous silica. *Chem. Eur. J.* **2013,** *19*, 10468-10472.

(29) Cheng, J.; Le Saux, G.; Gao, J.; Buffeteau, T.; Battie, Y.; Barois, P.; Ponsinet, V.; Delville, M. H.; Ersen, O.; Pouget, E.; Oda, R. GoldHelix: Gold Nanoparticles Forming 3D Helical Superstructures with Controlled Morphology and Strong Chiroptical Property. *ACS Nano* **2017,** *11*, 3806-3818.

(30) Gao, J.; Wu, W.; Lemaire, V.; Carvalho, A.; Nlate, S.; Buffeteau, T.; Oda, R.; Battie, Y.; Pauly, M.; Pouget, E. Tuning the Chiroptical Properties of Elongated Nano-Objects via Hierarchical Organization. *ACS nano* **2020**.

(31) Oda, R.; Huc, I.; Schmutz, M.; Candau, S.; MacKintosh, F. Tuning bilayer twist using chiral counterions. *Nature* **1999,** *399*, 566-569.

(32) Brizard, A.; Aimé, C.; Labrot, T.; Huc, I.; Berthier, D.; Artzner, F.; Desbat, B.; Oda, R. Counterion, temperature, and time modulation of nanometric chiral ribbons from gemini-tartrate amphiphiles. *J. Am. Ceram. Soc.* **2007,** *129*, 3754-3762.

(33) Sugiyasu, K.; Tamaru, S.-i.; Takeuchi, M.; Berthier, D.; Huc, I.; Oda, R.; Shinkai, S. Double helical silica fibrils by sol–gel transcription of chiral aggregates of gemini surfactants. *Chem. Commun.* **2002**, 1212-1213.

(34) Delclos, T.; Aime, C.; Pouget, E.; Brizard, A.; Huc, I.; Delville, M. H.; Oda, R. Individualized silica nanohelices and nanotubes: tuning inorganic nanostructures using lipidic self-assemblies. *Nano Lett.* **2008,** *8*, 1929-1935.

(35) Ji, X.; Copenhaver, D.; Sichmeller, C.; Peng, X. Ligand bonding and dynamics on colloidal nanocrystals at room temperature: the case of alkylamines on CdSe nanocrystals. *J. Am. Chem. Soc.* **2008,** *130*, 5726-5735.

(36) Boles, M. A.; Engel, M.; Talapin, D. V. Self-Assembly of Colloidal Nanocrystals: From Intricate Structures to Functional Materials. *Chem. Rev.* **2016,** *116*, 11220-11289.

(37) Chen, W.; Zhong, J.; Li, J.; Saxena, N.; Kreuzer, L. P.; Liu, H.; Song, L.; Su, B.; Yang, D.; Wang, K. Structure and Charge Carrier Dynamics in Colloidal PbS Quantum Dot Solids. *J. Phys. Chem. Lett.* **2019,** *10*, 2058-2065.

(38) Choi, J. J.; Luria, J.; Hyun, B. R.; Bartnik, A. C.; Sun, L.; Lim, Y. F.; Marohn, J. A.; Wise, F. W.; Hanrath, T. Photogenerated exciton dissociation in highly coupled lead salt nanocrystal assemblies. *Nano Lett.* **2010,** *10*, 1805-1811.

(39) Bodnarchuk, M. I.; Kovalenko, M. V.; Heiss, W.; Talapin, D. V. Energetic and entropic contributions to self-assembly of binary nanocrystal superlattices: temperature as the structure-directing factor. *J. Am. Chem. Soc.* **2010,** *132*, 11967-11977.

(40) Momper, R.; Zhang, H.; Chen, S.; Halim, H.; Johannes, E.; Yordanov, S.; Braga, D.; Blulle, B.; Doblas, D.; Kraus, T.; Bonn, M.; Wang, H. I.; Riedinger, A. Kinetic Control over Self-Assembly of Semiconductor Nanoplatelets. *Nano Lett.* **2020**, 20, 4102-4110.

(41) Weidman, M. C.; Smilgies, D. M.; Tisdale, W. A. Kinetics of the self-assembly of nanocrystal superlattices measured by real-time in situ X-ray scattering. *Nat. Mater.* **2016,** *15*, 775-781.

(42) Raino, G.; Becker, M. A.; Bodnarchuk, M. I.; Mahrt, R. F.; Kovalenko, M. V.; Stoferle, T. Superfluorescence from lead halide perovskite quantum dot superlattices. *Nature* **2018**, *563*,671-675.

(43) Chen, W.; Tang, H.; Li, N.; Scheel, M. A.; Xie, Y.; Li, D.; Körstgens, V.; chwartzkopf, M.; Roth, S. V.; Wang, K. Colloidal PbS quantum dot stacking kinetics during deposition via printing. *Nanoscale Horizons* **2020**, 5, 880-885.

(44) Gilmore, R. H.; Liu, Y.; Shcherbakov-Wu, W.; Dahod, N. S.; Lee, E. M.; Weidman, M. C.; Li, H.; Jean, J.; Bulović, V.; Willard, A. P. Epitaxial dimers and Auger-assisted detrapping in PbS quantum Dot solids. *Matter* **2019**, 1, 250-265.

(45) Yuan, X.; Hou, X.; Li, J.; Qu, C.; Zhang, W.; Zhao, J.; Li, H. Thermal degradation of luminescence in inorganic perovskite CsPbBr3 nanocrystals. *Phys. Chem. Chem. Phys.* **2017,** *19*, 8934-8940.

TOC image

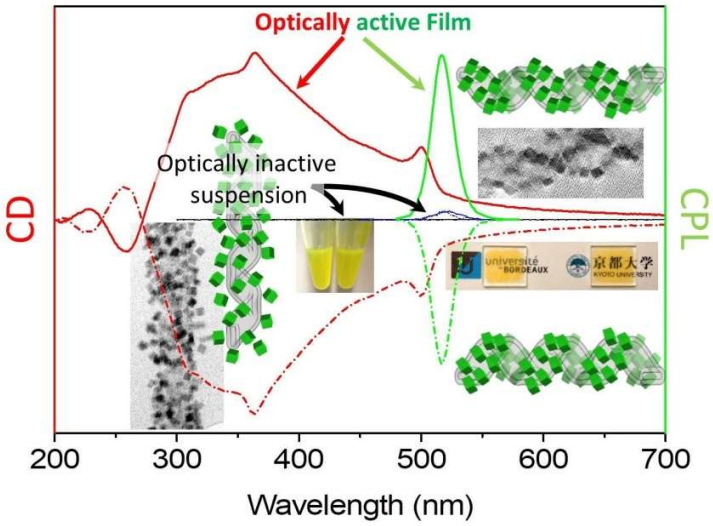

Perovskite $CsPbBr_3$ nanocrystals grafted on the surface of silica nanohelices. In toluene suspension, such PNC@silica nanohelices did not show observable optical activity. After drying on substrates to form films, strong CD and CPL signals were observed with the dissymmetric factor of > $6*10^{-3}$